Hindawi
Advances in High Energy Physics
Volume 2020, Article ID 4510897, 17 pages
https://doi.org/10.1155/2020/4510897

Research Article

Study of Di-Muon Production Process in *pp* Collision in CMS Data from Symmetry Scaling Perspective

Susmita Bhaduri, Anirban Bhaduri, and Dipak Ghosh

Deepa Ghosh Research Foundation, Kolkata 700031, India

Correspondence should be addressed to Susmita Bhaduri; susmita.sbhaduri@dgfoundation.in

Received 22 November 2019; Revised 1 January 2020; Accepted 7 March 2020; Published 26 March 2020

Academic Editor: Edward Sarkisyan-Grinbaum

An extensive knowledge of the dynamics of the process of *pp* collision serves as input to exhaustive theoretical models of strong interaction. This knowledge is also a baseline for a system to decipher the dynamics of *AA* collisions at relativistic and ultrarelativistic energies. Recent availability of di-muon data has triggered a spate of interests in revisiting strong interaction process, the study of which in detail is extremely important for enhancement of our understanding of not only the theory of strong interaction but also possible physics scenarios beyond the standard model. Apart from conventional approaches to the study of the dynamics of particle production in high-energy collision the present authors proposed a new approach with successful application in context of symmetry scaling in *AA* collision data from (ALICE-Collaboration, 2014) in the work (Bhaduri, S. et al., 2019) and *pp* collision data at 8TeV from (CMS-collaboration, 2017) in the work (Bhaduri, S. et al., 2019) and also in other numerous works with different collision data. This different approach essentially analyses fluctuation pattern from the perspective of symmetry scaling or degree of self-similarity involved in the process. This was done with the help of multifractal scaling analysis and also multifractal cross-correlation analysis using the single variable of pseudorapidity values of di-muon data taken out from the primary dataset of RunA(2011) and RunB(2012) of the *pp* collision at 7 TeV and 8 TeV, respectively, from (CMS-collaboration, 2016, 2017). High degree of persistent long-range cross-correlations (MF-DXA) exist between pseudorapidity-value and its corresponding azimuthal-value for different rapidity ranges. The different values of scaling exponents (across rapidity ranges and energies) signify that there may be multiple processes other than those conjectured, involved in the underlying dynamics of the production process of oppositely charged di-muons resulting in different kinds of scaling. Otherwise, the scaling exponents at different degrees would have remained the same across the rapidity ranges and also for different energies.

1. Introduction

In the recent past, fluctuation and correlation have been analyzed widely using novel methods of studying nonstatistical fluctuation which resulted in the better understanding of the dynamics of the pionisation process. The methods including the process of intermittency were introduced by Bialas and Peschanski [1] who have observed association between intermittency indices and anomalous fractal dimension [2, 3]. After that, the parameters of Gq moment and Tq moment [4–8] were introduced which were deduced from various methods based on fractal concepts. Then distinctive approaches of *detrended fluctuation analysis (DFA) and multifractal-DFA (MF-DFA)* [9, 10] were applied extensively for analyzing nonstationary, nonlinear properties of data series to investigate the long-range correlations inherent in the process of particle production [11–14]. Among various other contemporary works, self-similarity has been analyzed in the areas of particle physics which includes the production process of Jet and Top-quark in the experiments of Tevatron and LHC [15], the procedure of strangeness production in *pp* collisions at the RHIC [16] experiments, the phenomenon of proton spin and asymmetry inherent in jet production process [17] and the deciphering of the collective phenomena [18], and the process of establishment of the notion of self-similar symmetry of dark energy [19]. The

study of long-range cross-correlation between two nonstationary signals *detrended cross-correlation analysis (DXA)* had been presented by Podobnik and Stanley [20]. Wang et al. [21] introduced *multifractal-detrended cross-correlation analysis (MF-DXA)* by combining *MF-DFA* and *DXA* methods to examine higher degree of multifractal parameters of two cross-correlated series. MF-DXA method has been applied with substantially higher degree of accuracy in the analysis of the unrevealed cross-correlation in the various fields of physics, physiology finance, and power markets [20, 21] and also in the fields of particle physics [22].

The main aim of high-energy physics is to prove the existence of the creation of the QGP state, and also the study of the properties of this exotic state, by examining the final state of produced-hadrons, produced in huge numbers. Most of these final state particles may not be produced from the decay of the plasma directly, but rather they are produced or influenced by the hadronic cascade. Hence, studies of resonance states are of great importance because there is a variety of resonances, having very different lifespans, which signifies that these particles decay with differing probabilities in the hadronic stage, and therefore provide valuable information about that stage. We have performed the scaling analysis of the pseudorapidity space taken out from Pb-Pb VSD masterclass data at 2.76 TeV per nucleon pair from ALICE Collaboration [23] using both the method of complex network-based visibility graph and multifractal-DFA (MF-DFA) [9, 10], to study the prospective phase transition and the signature of QGP [24, 25]. We also studied multiplicity fluctuation process in nucleus-nucleus and hadron-nucleus interactions by applying complex network and chaos-based visibility graph methodology in quite a few recent works [22, 26–33]. These techniques have also been successfully applied to identify phase transitions in temperature-driven magnetization properties [34] and also in temperature-driven phase transition from liquid to vapour state [35]. In a recent study [36], different combinations of topological and kinematic input variables from the data of RunA(2011) of the *pp* collision at 7 TeV at CMS detector have been used, from which several ANNs (artificial neural networks) have been constructed, and then through comparison, the optimally configured ANN is selected .

The outcomes of the assessment of *pp* and *pA* systems should be used as a reference to validate the understanding of the processes which are expected to contribute to the dynamics of the process of di-muon production [37]. Moreover, apart from the analysis of *AA* collisions, an extensive knowledge of *pp* collisions is required both as an input to comprehensive theoretical models of strong interactions and also as a baseline to decipher the *AA* collisions at relativistic and ultrarelativistic energy levels. This has been of great interest in the area of theoretical and experimental physics. The process of soft particle generation from ultrarelativistic *pp* collisions is affected by the flavor distribution among the proton, quark hadronization, and baryon number transport. In the process of *AA* collisions, the magnitude of the spectrum of transverse momentum of charged particles in *pp* collisions serves as an important reference. A *pp* reference spectrum is required for *AA* collisions to probe for the effects of probable initial states of the collision. The multiplicity distribution of particles generated in *pp* collisions and the multiplicity dependence of various global event features serve as rudimentary observables which reflect the features of the underlying dynamics of the process of particle production. Therein lies the importance of analyzing the dynamics of di-muon production process in *pp* collisions. In this work, we have attempted DFA, MF-DFA, and MF-DXA for the scaling analysis of the rapidity and energy dependence of the di-muon production process.

The rest of the paper is structured in the following manner. The objective of the study is elaborated in Section 2. Section 3 describes the methods of analysis. Section 3.1 presents the algorithm of DFA and MF-DFA, and Section 3.2 presents the method of MF-DXA in detail and the importance of the parameters—the width of multifractal spectrum and the cross-correlation exponent. Section 4.1 describes the data in detail. Section 4.2 describes the details of our study and the deductions from the test results. Section 5 details the physical importance of the proposed parameters and their relevance with regards to the dynamics of the di-muon production process and finally comes the conclusion.

2. Goal of the Study

Using *pp* collisions at a center-of-mass energy of $\sqrt{S} = 7$ TeV, the analysis of the production process of exclusive $\gamma\gamma \longrightarrow \mu^+\mu^-$ was carried out by the ATLAS and CMS collaborations [38]. A latest review work has been reported about the complexities involved in resonance production process for different high-energy collisions like *pp*, *pA*, and *AA* collisions at LHC(using data from ALICE collaboration), to analyze the complexity and eventually explain the inherent dynamics of the particle production process and the properties of the generated particles for the different collision system [39]. We have elaborated in Section 1 how after few successful ventures by the present authors in the field of analyzing the pionisation process in high-energy interaction using chaos-based procedures and being motivated by the different attempts reported to investigate the dynamics of the generation process of di-muon pairs in [39], we have attempted to revisit the di-muon production process in hadron-hadron interactions. We have proposed to implement the chaos-based methods of DFA, MF-DFA, and MF-DXA to analyze the energy and rapidity dependence of di-muon production process by utilizing a single variable of pseudorapidity values of di-muon data taken out of the primary dataset of RunA(2011) and RunB(2012) of the *pp* collision at 7 TeV and 8 TeV, respectively, from CMS collaboration [40, 41]. The rapidity and energy dependence of the process are examined by means of fundamental scaling parameter signifying the degree of symmetry scaling or scale-freeness in the di-muon production process, extracted by the proposed method.

(1) All these rigorous methods provide the information from the deepest level about the particle production process from the emergent di-muons produced from the *pp* collisions at 7 TeV and 8 TeV from CMS collaboration [40, 41].

(2) The study reveals that pseudorapidity spaces corresponding to different range of pseudorapidity values are highly scale free and possess multifractal characteristics. They also reveal how the scaling pattern changes from one rapidity range to another and also from one range of energy level to another

(3) For different rapidity range and at two different levels of energy, differences in the values of scaling exponent signify that there are multiple processes involved in the production process of oppositely charged di-muons which give rise to different kinds of scaling

Traditionally invariant-mass/transverse-momentum methods were used to probe various resonance states in high-energy collision. Apart from the J/Ψ peak observed in their invariant-mass spectrum, there can be existence of other upsilon states and other processes in principle contributing to the di-muon continuum due to open charm and open beauty decays. One may select different ranges of invariant mass by examining the pattern of invariant-mass spectrum of the events producing di-muons. For each such range, the pseudorapidity spaces corresponding to the produced di-muons would be extracted, and then for each of the spaces, the proposed scaling analysis may be done for different ranges of rapidity and energy. Any substantial change in scaling behavior indicated by the width of MF-DFA spectrum and the degree of multifractal cross-correlation may be attributed to the occurrence of different kinds of resonance states from which di-muons are produced in pp collisions. This may act as basic input for studying similar resonance production in pp collisions at higher energy and also for pA and AA collisions.

3. Method of Analysis

We have elaborated the multifractal-detrended fluctuation analysis (MF-DFA) method [9, 10, 42] used to calculate the Hurst exponent and the width of the multifractal spectrum. We have extracted these parameters for analyzing the fluctuation of data series extracted from the experimental data as elaborated in Section 4.1.

3.1. MF-DFA Method

(1) Here, we denote the experimental data series as $x(i)$ for $i = 1, 2, \cdots, N$, where N = number of points. The average of this series is computed as $\bar{x} = 1/N \sum_{i=1}^{N} x(i)$. Then, the collective deviation series for $x(i)$ is calculated as

$$X(i) \equiv \sum_{k=1}^{i} [x(k) - \bar{x}], \; i = 1, 2, \cdots, N. \tag{1}$$

This deduction of the average ($\bar{x}$) from the input data series is a conventional method of eliminating noise from the input data series. The result of this subtraction would be removed by the detrending process in the fourth step.

(2) $X(i)$ is then divided into N_s nonoverlapping segments, with $N_s \equiv \text{int}\,(N/s)$ and s as the length of the segment. In this experiment, s ranges from 16 (minimum) to 1024 (maximum) value in log scale

(3) For each s, a particular segment is denoted by $\nu (\nu = 1, 2, \cdots, N_s)$. Least-square fitting is performed for each segment to derive the local trend for that specific segment [9]. $x_\nu(i)$ denotes the least-square fitted polynomial for the segment ν in series $X(i)$. $x_\nu(i)$ is computed according to the equation $x_\nu(i) = \sum_{k=0}^{m} C_k (i)^{m-k}$, with C_k as the kth coefficients of the fitted polynomial of degree m. Different kinds of fitting—linear, quadratic, cubic, or higher m-order polynomial—may be used [10, 42]. In this experiment, linear least-square fitting is applied with $m = 1$

(4) Now, to detrend the data series, the least-square fitted polynomial is subtracted from the data series. There is existence of slow-varying trends in natural data series. In order to extract the scale invariant structure of the dissimilarity around the trend, detrending is necessary. For each value of s and segment $\nu \in 1, 2, \cdots, N_s$, detrending is executed by deducting the least-square fit $x_\nu(i)$ from the specific portion of the data series $X(i)$, for the segment ν to calculate the variance which is denoted by $F^2(s, \nu)$ computed as

$$F^2(s, \nu) \equiv \frac{1}{s} \sum_{i=1}^{s} \{X[(\nu - 1)s + i] - x_\nu(i)\}^2, \tag{2}$$

with $s \in 16, 32, \cdots, 1024$ and $\nu \in 1, 2, \cdots, N_s$.

(5) Next, the q^{th} order function of fluctuation, denoted by $F_q(s)$, is computed by averaging the values of $F^2(s, \nu)$ over all the segments (ν) produced for each $s \in 16, 32, \cdots, 1024$ and for a specific q, as

$$F_q(s) \equiv \left\{ \frac{1}{N_s} \sum_{\nu=1}^{N_s} \left[F^2(s, \nu) \right]^{q/2} \right\}^{1/q}. \tag{3}$$

Here, $q \neq 0$ as in that case $^{1/q}$ would blow up. In this experiment q varies from (−5) to (+5). For $q = 2$, computation of $F_q(s)$ would sum up to conventional method of detrended fluctuation analysis (DFA) [9].

(6) The above steps are repeated for various values of $s \in 16, 32, \cdots, 1024$, and it is observed that for a particular q, $F_q(s)$ rises in value with increasing s. If the data series is long-range power correlated, then $F_q(s)$ vs s for a specific q will display power-law behavior

$$F_q(s) \propto s^{h(q)}. \tag{4}$$

If this type of scaling exists, then $\log_2[F_q(s)]$ depends on $\log_2 s$ in a linear fashion, where $h(q)$ is the slope which is dependent on q. $h(2)$ is alike to the so-called *Hurst exponent* [42]. So $h(q)$ is defined as the generalized Hurst exponent.

(7) The scaling pattern of the variance $F^2(s, v)$ is the same for all segments in case of a monofractal series. In other words, the averaging of $F^2(s, v)$ would show uniform scaling behavior for various values of q, and hence, $h(q)$ becomes independent of q for monofractals.

But if large and small fluctuations in the series have varying scaling pattern, then $h(q)$ becomes substantially dependent on q. In these cases, for positive values of q, $h(q)$ delineates the scaling pattern of the segments with large fluctuations, and for negative values of q, $h(q)$ describes scaling behavior of the segments with smaller fluctuations. The generalized Hurst exponent $h(q)$ for a multifractal data series is associated with the classical multifractal scaling exponent $\tau(q)$ according to

$$\tau(q) = qh(q) - 1. \tag{5}$$

(8) As multifractal series have numerous Hurst exponents, so $\tau(q)$ depends nonlinearly upon q [43]. The singularity spectrum, here denoted by $f(\alpha)$, is associated with $h(q)$ as

$$\alpha = h(q) + qh'(q), f(\alpha) = q[\alpha - h(q)] + 1. \tag{6}$$

Here, the singularity strength is denoted by α, and $f(\alpha)$ describes the dimension of the subset series denoted by α. Different values of $f(\alpha)$ for different α results into multifractal spectrum of $f(\alpha)$ which is an arc, and for this spectrum, the gap between the maximum and minimum values of α is the *width of the multifractal spectrum* or the measurement of the multifractality of the input data series.

(9) For $q = 2$, if $h(q)$ or $h(2) = 0.5$, no correlation exists in the data series. There is persistent long-range cross-correlations in the data series, which means a large value in the series is presumably to be followed by another large value in the series, if $h(2) > 0.5$, whereas for $h(2) < 0.5$, there would be antipersistent long-range correlations which implies that a large value would probably be followed by a small value in the series and vice versa.

3.2. MF-DXA Method. Wang et al. [21] have introduced *MF-DXA* method based on the *MF-DFA* method [10, 42] and analyzed the cross-correlation between two nonstationary series quantitatively. The broad steps for the *MF-DXA* method are as follows.

(1) Let $x(i)$ and $y(i)$ be two data series for $i = 1, 2, \cdots, N$, of length N. The mean of these series is calculated as $\bar{x} = 1/N\sum_{i=1}^{N} x(i)$ and $\bar{y} = 1/N\sum_{i=1}^{N} y(i)$, respectively. Then, accumulated deviation series for $x(i)$ and $y(i)$ are calculated as per equation (1) and denoted by $X(i)$ and $Y(i)$, respectively. Both $X(i)$ and $Y(i)$ are divided into N_s nonoverlapping segments, where $N_s = \text{int}(N/s)$, s is the length of the segment. In our experiment, s varies from a minimum of 16 to a maximum of 512 value in log scale

(2) For each s, we denote a particular segment by $v (v = 1, 2, \cdots, N_s)$. Here, $x_v(i)$ and $y_v(i)$ denote the least-square fitted polynomials for the segment v in $X(i)$ and $Y(i)$, respectively. $x_v(i)$ and $y_v(i)$ are calculated as per the equations $x_v(i) = \sum_{k=0}^{m} C_{xk}(i)^{m-k}$ and $y_v(i) = \sum_{k=0}^{m} C_{yk}(i)^{m-k}$, where C_{xk} and C_{yk} are the k^{th} coefficients of the fit polynomials with degree m. For this experiment, m is taken as 1 [21].

For each s and segment v, $v = 1, 2, \cdots, N_s$, detrending is done by subtracting the least-square fits $x_v(i)$ and $y_v(i)$ from the part of the data series $X(i)$ and $Y(i)$, respectively, for the segment v. The covariance of the these residuals, denoted by $f_{xy}^2(s, v)$ for a particular s and v, is then calculated as follows.

$$f_{xy}^2(s, v) = \frac{1}{s}\sum_{i=1}^{s}\{X[(v-1)s + i] - x_v(i)\} \times \{Y[(v-1)s + i] - y_v(i)\}, \tag{7}$$

for each segment v, $v = 1, 2, \cdots, N_s$.

(3) Then, the q^{th} order detrended covariance, denoted by $F_{xy}(q, s)$, is calculated by averaging $f_{xy}^2(s, v)$ over all the segments (v) generated for a particular s and q, as per the equation below [10, 21, 42].

$$F_{xy}(q, s) = \left\{\frac{1}{N_s}\sum_{v=1}^{N_s}\left[f_{xy}^2(s, v)\right]^{q/2}\right\}^{1/q}. \tag{8}$$

Here, $q \neq 0$ because in that case, $1/q$ would blow up.

(4) The above process is repeated for different values of $s \in 16, 32, \cdots, 512$, and it can be seen that for a specific q, $F_{xy}(q, s)$ increases with increasing s. If the series are long-range power correlated, the relation between $F_{xy}(q, s)$ versus s for a particular q will show power-law behavior as below [21].

$$F_{xy}(q, s) \propto s^{h_{xy}(q)}. \tag{9}$$

If this kind of scaling exists, $\log_2[F_{xy}(q, s)]$ would depend linearly on $\log_2 s$, where $h_{xy}(q)$ is the slope

and represents the degree of the cross-correlation between the data series $x(i)$ and $y(i)$.

In general, $h_{xy}(q)$ depends on q. q ranges from negative to positive values. For $q = 2$, the method is referred as the so-called method of *DXA* [21].

(5) As confirmed from several experiments done by Wang et al. [21], if $h_{xy}(q) = 0.5$, there is no cross-correlation. Further, if $h_{xy}(q) > 0.5$, there are persistent long-range cross-correlations, where the large value of one variable, which is in this study the η values, is likely to be followed by a large value of another variable, which is the corresponding ϕ values, in the series, whereas in case of $h_{xy}(q) < 0.5$, there are antipersistent long-range cross-correlations, where a large value of one variable is most likely to be followed by a small value and vice versa in the series

(6) $h_{xy}(q)$ for $q = 2$, i.e., $h_{xy}(2)$, is the *DXA* exponent. As per Podobnik and Stanley, the cross-correlation exponent between two nonstationary series, denoted by γ_i, is calculated as per the equation $\gamma_i = 2 - 2\{h_{xy}(2)\}$ [20]. For uncorrelated data series, $\gamma_i = 1$, the lower the value of γ_i, the more correlated the data series are

4. Experimental Details

The datasets for the proposed analysis are taken out from two publicly available experimental primary datasets from CMS collaboration. The details of the data is given in Section 4.1, and the complete method of the experiment is explained in step by step in Section 4.2.

4.1. Data Description. The primary dataset of the *pp* collision at 8 TeV in AOD format from RunB of 2012 [40] and another dataset of *pp* collision at 7 TeV in the same AOD format from RunA of 2011 [41] of the CMS collaboration are taken as the source datasets for this experiment. The run numbers which are selected and qualified by CMS to be processed along with the appropriate parameters for generation of the collision datasets are provided in the links—*link1* and *link2* for 8 TeV and 7 TeV, respectively. These datasets are made available for experiment. We have extracted the pseudorapidity-η space and corresponding azimuthal-ϕ space for the generated di-muons from these runs qualified by CMS from the primary datasets in the following formats—text (.txt) and .root format. In this analysis, we have utilized these pseudorapidity space and the corresponding azimuthal space from the text (.txt) file.

4.2. Data Analysis and Results

(1) The pseudorapidity-η space for each of the datasets for 8 and 7 TeV extracted from the primary datasets of the CMS collaboration as described in Section 4.1 is divided into the following 5 ranges of η values

(a) −2.5 to −1.5

(b) −1.5 to −0.5

(c) −0.5 to 0.5

(d) 0.5 to 1.5

(e) 1.5 to 2.5

For all the 5 ranges, the η values are extracted from the full-phase space of the two source datasets and mapped to data series. The data series is plotted with the X-axis denoting the sequence number of η values and the Y corresponds to the η values corresponding to the sequence number as in the X-axis.

For each of these data series, the following values are calculated.

(i) The width of the multifractal spectrum

(ii) Degree of cross-correlation between the η space and their corresponding ϕ space

(2) For each of the 10 datasets (5 for 8 TeV and 5 for 7 TeV datasets) created for the 5 ranges of pseudorapidity values, as specified in Step 1, the multifractal analysis is done and the width of multifractal spectrum is calculated as per the method elaborated in Section 3.1

The q^{th} order detrended variance $F_q(s)$ is calculated as per equation (3) in the Step 5 of the MF-DFA methodology as described in Section 3.1. Figures 1(a) and 1(b) show the $\log_2[F_q(s)]$ vs $\log_2[s]s$ trend for $q = -5, 0, 5$, extracted for a particular range of η values for 8 and 7 TeV datasets, respectively.

Their linear trend confirms the power-law behavior of $F_q(s)$ versus s for all the values of q. Similar calculation is done for all the η ranges for both 8 and 7 TeV datasets, and similar trend is observed.

(3) For each of the η-data series corresponding to the ranges specified in Step 1, a randomized version of data is produced and widths of the multifractal spectrum are calculated as per the same methodology elaborated in Section 3.1. The calculated values of the parameters are compared to those for the experimental data. In Figures 2(a) and 2(b), the widths of the multifractal spectrum of the original datasets and their randomized versions calculated for one of the ranges η values are shown for 8 and 7 TeV datasets, respectively. The below points must be noted for the shape and widths of the multifractal spectrum of the original datasets and their randomized versions

(i) The shape of the multifractal spectrum does not necessarily have to be symmetric. The spectrum might have either a right or a left truncation that arises from the consistent/(almost

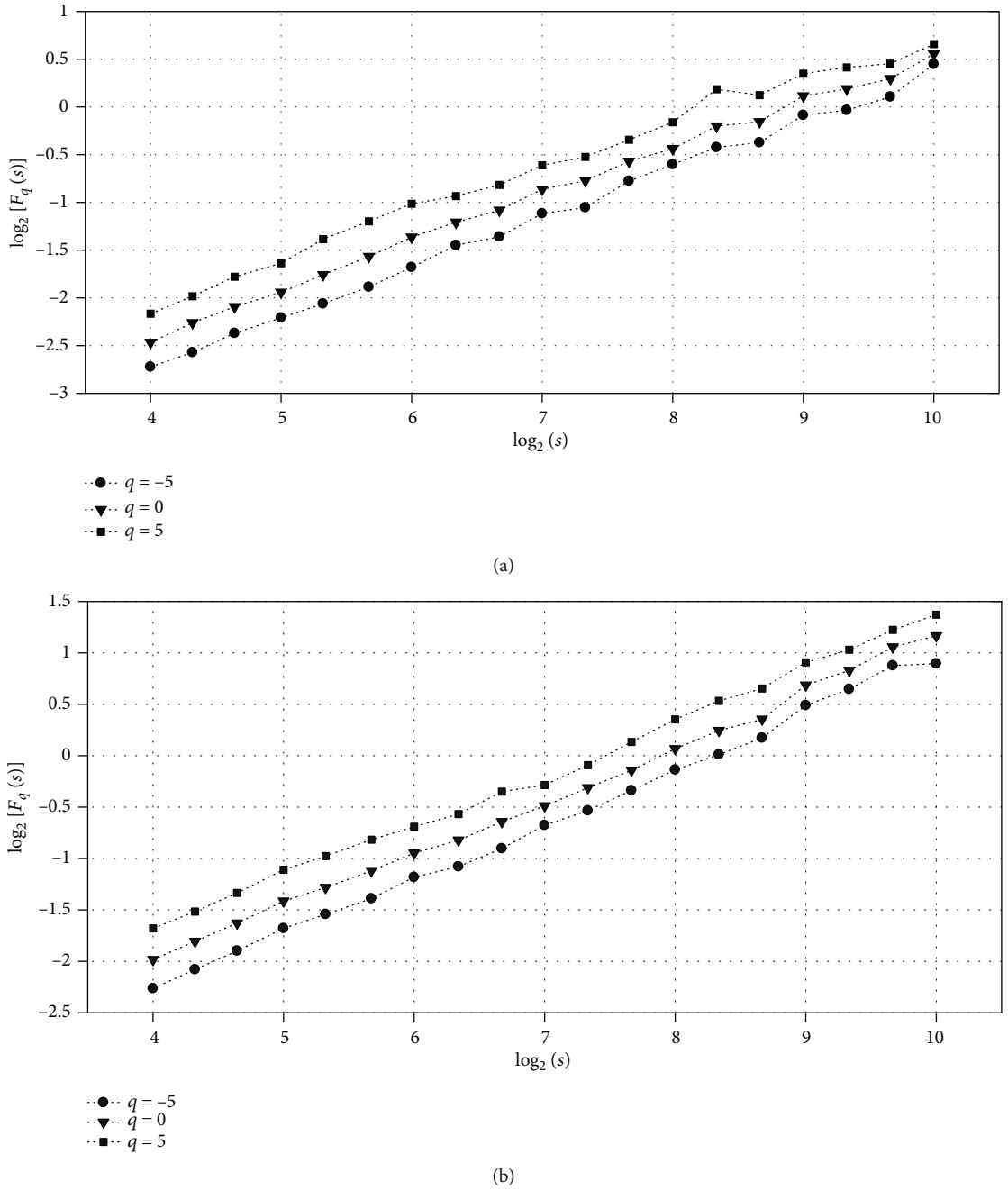

FIGURE 1: Trend of $\log_2[Fq(s)]$ vs $\log_2[s]s$ for $q = -5, 0, 5$, extracted for a particular range of η (a) for 8 TeV dataset and (b) for 7 TeV dataset.

constant) trend of Hurst exponents for positive or negative values of qs. The consistent trend of q^{th} order Hurst exponent signifies that the q^{th} order RMS (calculated as per the equations in Step 5 and Step 6 of Section 3.1) is not much sensitive to the extent of the local fluctuations

(ii) The width and trend of multifractal spectrum between the original and the randomized version of the particular η-space for 8 TeV dataset shown in Figure 2(a) shows that the spectrum for the randomized version has a long right tail which signifies that the series have a multifractal structure not much affected by the local fluctuations with large magnitudes

(iii) Whereas the multifractal spectrum calculated for the original and the randomized version of the η-space for the same range of η values for 7 TeV dataset shown in Figure 2(b) shows that the spectrum for the randomized version has a long left tail, which means that the randomized series is not much sensitive to the local fluctuations with small magnitudes.

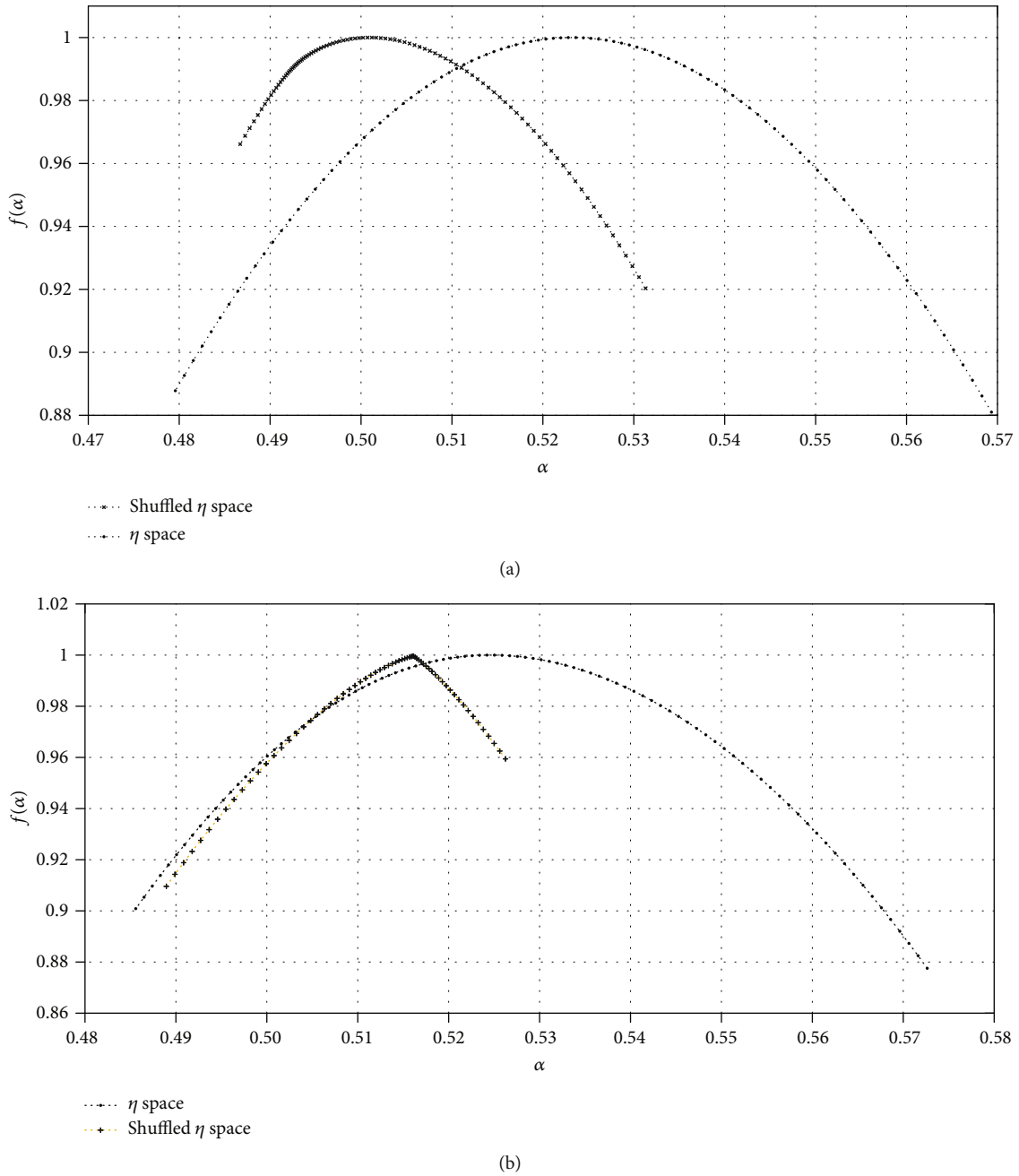

FIGURE 2: Comparison of the trend of different values of $f(\alpha)$ versus α between the original and the randomized version of the η space for a particular range of η values for (a) 8 TeV dataset and (b) 7 TeV dataset.

(iv) If the source data is long-range correlated, that is eradicated by the randomization process, and the data should start to become uncorrelated. This makes the multifractal spectrum or the scaling pattern of randomized series insensitive to the local fluctuations with large or small magnitudes, which is not the case with the actual experimental data. Hence, it results in the different widths of multifractal spectrum calculated the randomized version from those for the original version. Moreover, for two completely different experimental datasets the randomized data may be different with regards to peak, shape, and trend. The width of the multifractal spectrum has normally been less for the randomized data than the one for the experimental data

(v) The main conclusion comes from the fact that the values of the width of the multifractal spectrum calculated experimental data being significantly different from shuffled ensembles

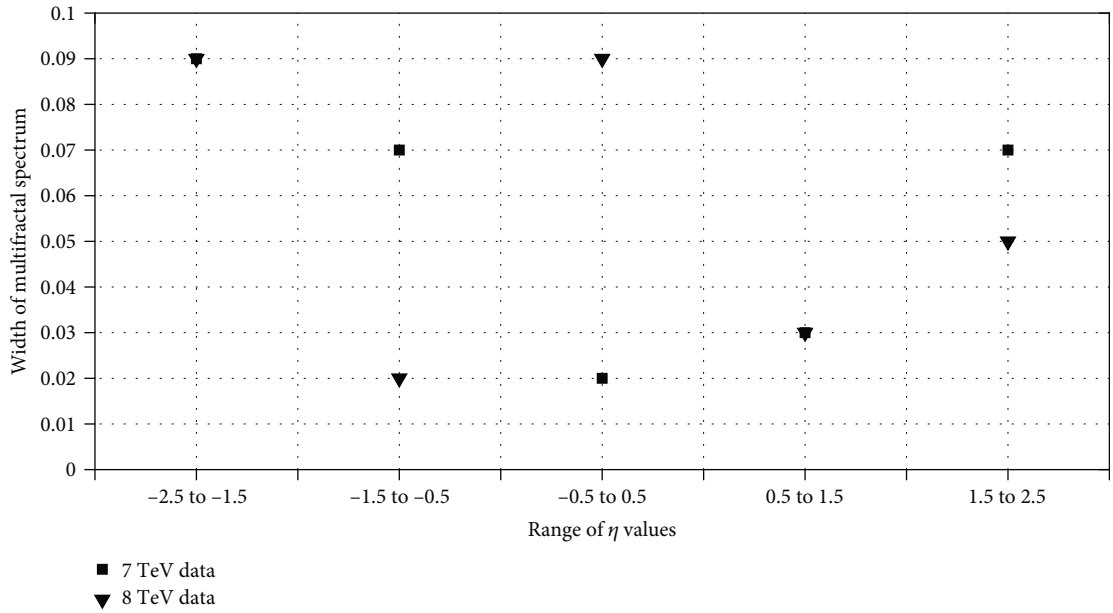

Figure 3: Comparison of the widths of the multifractal spectrum generated η spaces for all the 5 ranges of η values for 7 and 8 TeV datasets.

essentially confirms that the *degree* of scale-freeness is indicative of the dynamics inherent in the di-muon production process, and this *degree* of scale-freeness may be indicative of different processed responsible for di-muon production even beyond standard model (SM).

(vi) It is evident from the figures that the widths of the multifractal spectrum of the original datasets and their randomized versions differ substantially for both energies. Similar trend is observed from the comparison of the original and the randomized version of the 5 ranges of η values for both 8 and 7 TeV datasets

The comparison of the widths of the multifractal spectrum generated for the η spaces for all the 5 ranges of η values for 7 and 8 TeV datasets with respect to their rapidity and energy dependence is shown in Figure 3. It should be noted that:

(i) The comparison of the width of the multifractal spectrum of $f(\alpha)$, denoted by the difference between the maximum and minimum values of α, between the original and the randomized version of the η space for both energy ranges confirm the mutifractality of the original η spaces

(ii) For the 2nd, 3rd, and 5th range of η values, the widths of multifractal spectrum is substantially different between the energy ranges

(iii) For both 7 and 8 TeV the 1st and 4th range of η-space display minimum or no difference with respect to multifractality

Table 1: Comparison of the widths of the multifractal spectrum generated η spaces for all the 5 ranges of η values for 7 and 8 TeV datasets, between the original and the randomized version.

η ranges	MF-DFA spectrum width			
	8 TeV		7 TeV	
	Original	Random	Original	Random
−2.5 to −1.5	0.09	0.06	0.09	0.04
−1.5 to −0.5	0.02	0.01	0.07	0.02
−0.5 to 0.5	0.09	0.04	0.02	0.04
0.5 to 1.5	0.03	0.02	0.03	0.04
1.5 to 2.5	0.05	0.04	0.07	0.06

(iv) The degree of multifractality is found to be the least for 2nd and 3rd range for 8 and 7 TeV data, respectively

Table 1 details the widths of the multifractal spectrum of the original datasets and their randomized versions for all the 10 datasets (5 for 8 and 5 for 7 TeV) corresponding to the η values. The values of the width of MF-DFA spectrum, essentially is an indicator of inherent symmetry and scale-freeness (different at different energy and rapidity ranges) with which the produced di-muons create the signatures in terms of η values. The values of these parameters in experimental data being significantly different from shuffled ensembles confirm that this inherent symmetry and degree of scale-freeness is never the outcome of randomization process but is indicative of the dynamics involved in the di-muon production process.

(4) For each of the 10 datasets (5 for 8 and 5 for 7 TeV) of η values extracted for the ranges specified in

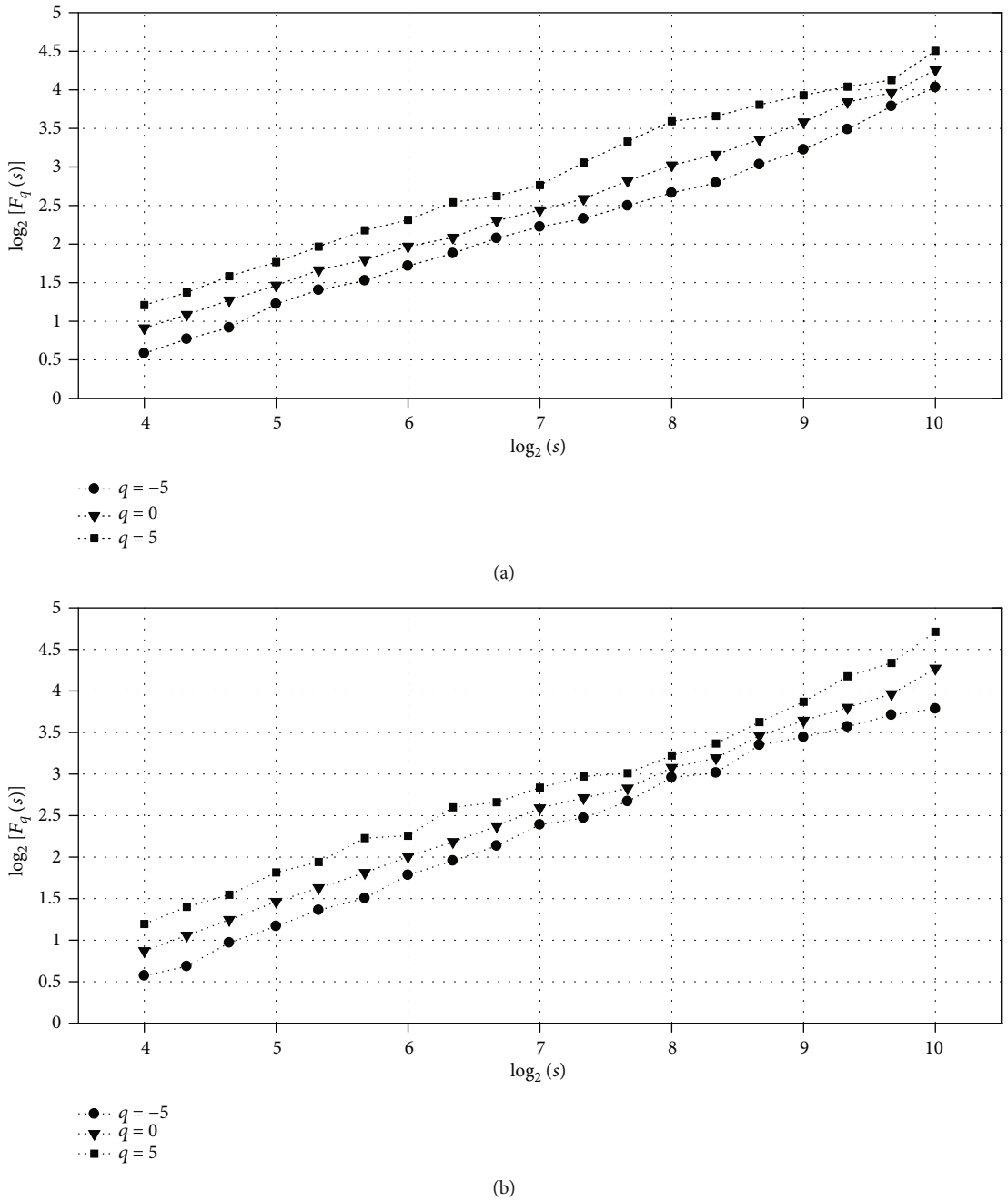

FIGURE 4: Trend of $\log_2[F_q(s)]$ vs $\log_2[s]s$ for $q = -5, 0, 5$, analyzed for the ϕ space corresponding to the η space for (a) 8 TeV dataset, as shown in Figure 1(a), and (b) 7 TeV dataset, as shown in Figure 1(b).

Step 1, the corresponding azimuthal-ϕ space is also extracted. The 10 corresponding ϕ space is sorted in the ascending order and then mapped into data series. They in turn are mapped into a two-dimensional space with their sequence along the X-axis and the corresponding values of ϕ along the Y-axis

(5) For the 10 ϕ spaces (5 for 8 and 5 for 7 TeV), the q^{th} order detrended variance $F_q(s)$ is analyzed as per equation (3) in Step 5 of the MF-DFA methodology as described in Section 3.1. Figures 4(a) and 4(b) show the $\log_2[F_q(s)]$ vs $\log_2[s]s$ trend for $q = -5, 0, 5$, extracted for corresponding ϕ values for the same range of η values for which the same trend is shown in Figures 1(a) and 1(b) for 8 and 7 TeV datasets, respectively

It is to be noted that the linear trend confirms the power-law behavior of $F_q(s)$ versus s for all the values of q for the ϕ spaces. The same analysis is done for all the ϕ spaces corresponding to the η ranges for both 8 and 7 TeV datasets, and a similar trend is observed.

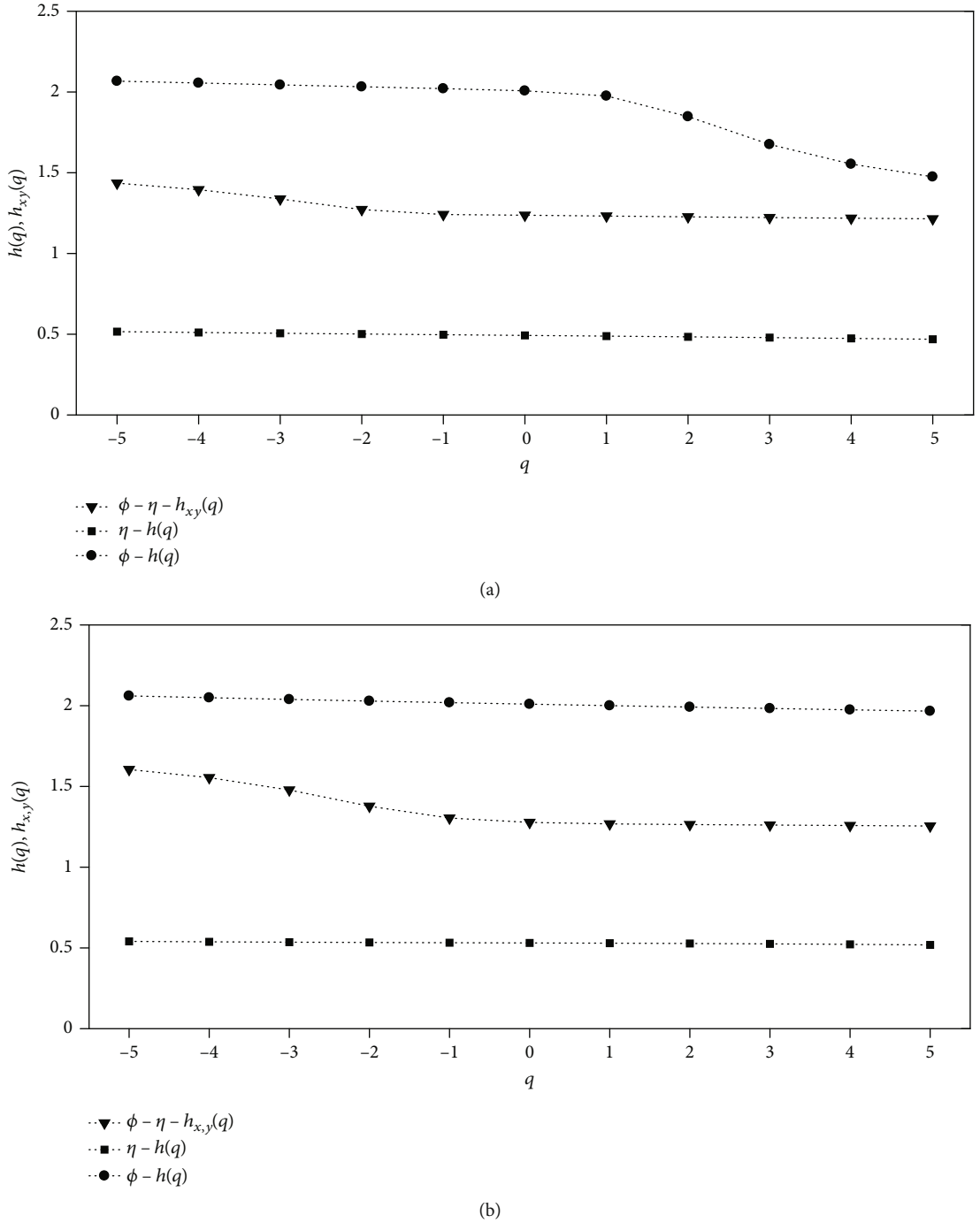

FIGURE 5: Trend of $h(q)$ and $h_{x,y}(q)$ versus q for $q = -5, -4, \cdots, 5$, calculated for a particular range of η values and their corresponding ϕ values for (a) 8 TeV dataset and (b) 7 TeV dataset.

(6) Multifractal cross-correlation analysis is done as per the method described in Section 3.2 between the 10 pairs of datasets (5 for 8 TeV and 5 for 7 TeV), one being the sorted ϕ values and the other being the corresponding η values. The trend of generalized Hurst exponent $(h(q))$ for different order (q) is analyzed for all the 10 pairs of η and ϕ datasets as per the process described in Section 3.1. Along with that, for the same pairs of datasets the degree of cross-correlation$(h_{x,y}(q))$ for different order (q) is analyzed as per the methodology described in Section 3.2. The trend of $h(q)$ and $h_{x,y}(q)$ versus q for the particular sample pair of η and ϕ space for which trends of $\log_2[F_q(s)]$ vs $\log_2[s]s$ are shown in Figure 1(a) (η space) and Figure 4(a) (ϕ space) for 8 TeV dataset and Figure 1(b) (η space) and Figure 4(b) (ϕ space) for 7 TeV dataset is shown in Figures 5(a) and

5(b) for 8 and 7 TeV datasets, respectively. The values are shown in the figures for $q = -5, -4, \cdots, 5$. It should be noted that:

(i) As shown in Figures 5(a) and 5(b), the trend of dependence of $h(q)$ on q for individual η and ϕ spaces confirm their multifractality and the same for $h_{x,y}(q)$ on q for the same pair of η and ϕ spaces confirm their cross-correlation for both 8 and 7 TeV datasets

(ii) Figures 5(a) and 5(b) show that $h(q)$ decreases at a lower rate for the increasing values of negative qs for both φ and η data ranges in both energies of 8 and 7 TeV. This signifies that for negative values of q, the q^{th} order RMS (calculated as per the equations in Step 4 and Step 5 of Section 3.1) is not much sensitive to the local fluctuations with small magnitudes for the datasets (ϕ and η) for both energies

However, for the ϕ data series corresponding to the particular range of η at 8 TeV, $h(q)$ decreases at a higher rate for positive values of q than the corresponding ones calculated for the same range of η at 7 TeV. This means, in this case, $h(q)$ is a bit more affected by the local fluctuations with large magnitudes, resulting in higher rate of decrease for $h(q)$ with increasing order of positive q for the ϕ data series of 8 TeV than the corresponding one for 7 TeV data. This has happened because there may exist fluctuations with comparatively large magnitude for the φ data series for higher energy—8 TeV than the one for 7 TeV.

(i) It is further observed in Figures 5(a) and 5(b) that $h_{x,y}(q)$ (calculated as per the equation in Step 4 of Section 3.2) for multifractal cross-correlation changes almost at the same rate for both 8 and 7 TeV energies. It should be noted that the maximum and minimum values of $h_{x,y}(q)$ for 8 and 7 TeV are different; however, the change of $h_{x,y}(q)$ with the increasing values of q is almost the same. Although for 8 TeV, there is higher rate of decrease for $h(q)$ with increasing order of positive qs for the ϕ data series than the corresponding one for 7 TeV data, resulting from possible higher magnitude of fluctuation for ϕ data series, that decreasing trend gets nullified while calculating the covariance of ϕ data series and corresponding η data series at 8 TeV energy. Hence, the trend of $h_{x,y}(q)$ with the increasing values of q is almost the same for both energies. However, this has resulted in the lower ranges of the values of degree of cross-correlation $h_{x,y}(q)$ for 8 TeV, making them less cross-correlated

(ii) For $q = 2$, both $h(q)$ and $h_{x,y}(q)$ are >0.5 and for ϕ space $h(q)$ is much higher than that for the corresponding η space

(iii) Also, $h_{x,y}(q)$ is much higher than 0.5 for the pair of datasets for $q = 2$. This suggests the presence of long-range correlation and persistence in both spaces

(iv) Moreover, there is a drop in the value of $h_{x,y}(q)$ around $q = -1$. In most of the previous works, it has been shown that there exists similar trend of $h_{x,y}(q)$ or the degree of cross-correlation with increasing values of order or q, as seen in the present analysis

(v) Similar analysis has been done for all the 10 pairs of datasets, and similar trend is observed for all of them

(7) Figures 6(a) and 6(b) show the comparison of the trend of different values of $f(\alpha)$ versus α for the same η, ϕ spaces and the same trend calculated for their cross-correlation, for 8 and 7 TeV datasets, respectively

(i) For both energy ranges, width of the cross-correlation curve is the maximum, followed by the width of the multifractal spectrum of the ϕ space and then that of the η space

(ii) Again, similar trend is observed for all the pairs of datasets in this experiment. The more wide the spectrum is, the more degree of multifractality is inherent in the data series

(8) The q^{th} order detrended covariance $F_{xy}(q, s)$ is calculated for a particular range of η values and their corresponding ϕ values as per the Step 4 of the MF-DXA methodology described in Section 3.2, and the trend of $\log_2[F_{xy}(q, s)]$ vs $\log_2[s]$ for $q = -5, 0, 5$ is shown in Figures 7(a) and 7(b) for 8 and 7 TeV datasets, respectively

(i) Their linear trend (more prominent for the values of $q > 0$) confirms the power-law behavior of $F_{xy}(q, s)$ versus s for all the values of q

(ii) Similar calculation is done for all the η ranges and their corresponding ϕ spaces, for both 8 and 7 TeV datasets, and similar trend is observed

As explained in Step 5 of the MF-DXA methodology described in section 3.2, here, $h_{xy}(q) > 0.5$ implies that there are persistent long-range cross-correlations, where a large value in ϕ space is likely to have an equally large corresponding η value. The higher the value of $h_{xy}(q)$, the higher the cross-correlation. Figures 7(a) and 7(b) show how the q^{th}

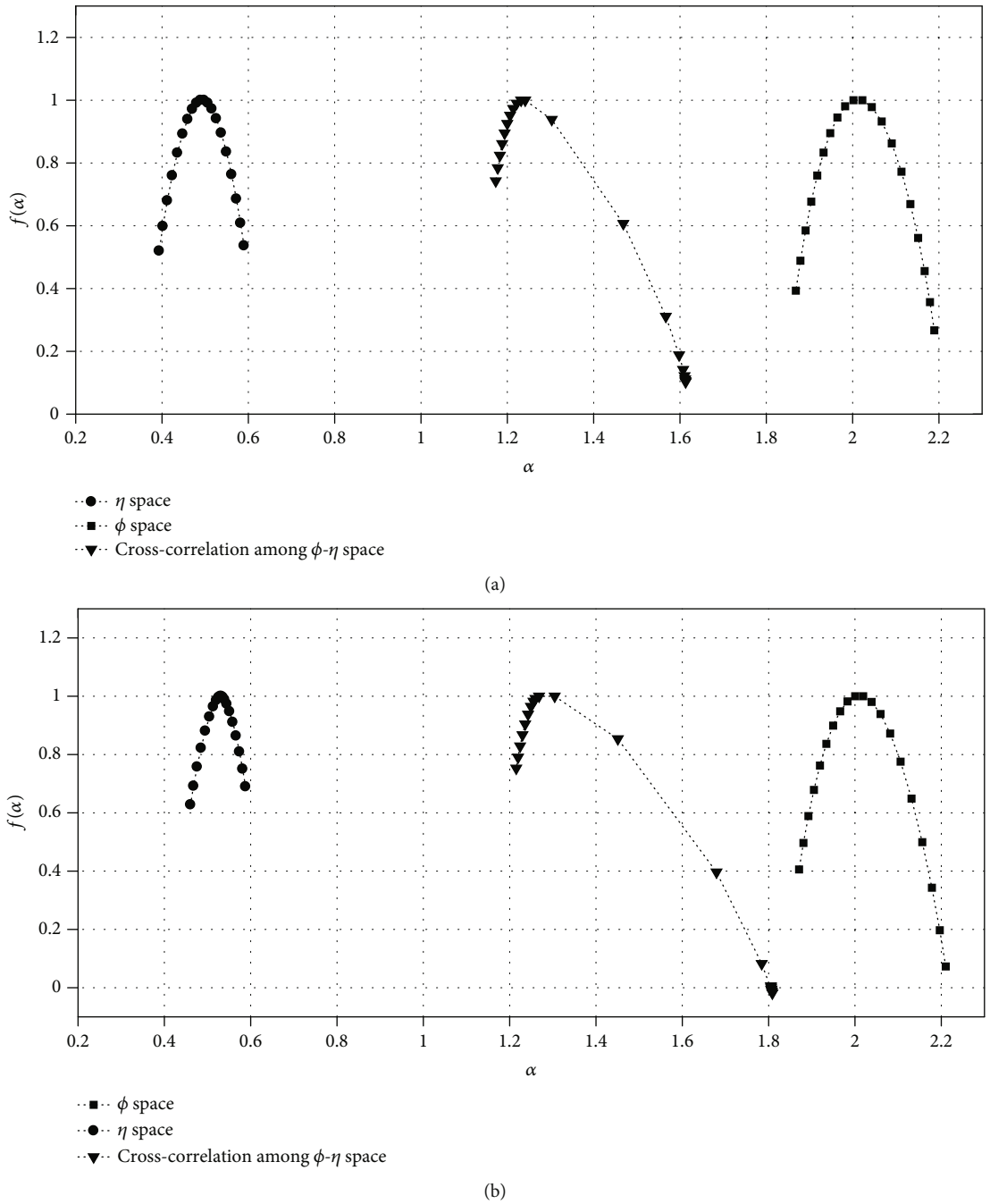

Figure 6: Comparison of the trend of different values of $f(\alpha)$ versus α among the same η, ϕ spaces and the same trend calculated for their cross-correlation, for the (a) 8 TeV dataset and (b) 7 TeV dataset.

order detrended covariance or $F_{xy}(q,s)$ varies with increasing values of scale (s) in log scale. The straight line fitting of $F_{xy}(q, s)$ versus s in log scale is shown in the figures and the relevant power-law coefficients or degree of cross-correlations ($h_{xy}(q)$) are also shown in the fitting equations in the diagram. It is evident from the figures that for negative values of q, degree of cross-correlation is higher than that for positive values of q. Covariance of small magnitudes are reflected more prominently for negative values of q, which signifies that the average cross-correlation between φ spaces and their corresponding η spaces fluctuates more for the values of $q < 0$ and gives rise higher value of $h_{xy}(q)$. This fluctuation becomes lesser as q increases from $q = -5, -4, \cdots, -1$. For positive values of q ($q \geq 0$), the q^{th} order detrended covariance starts to fluctuate very less and gives rise to lesser values of $h_{xy}(q)$. Hence, the value of $h_{xy}(q)$ also changes more for $q < 0$ than for $q > 0$. This different degree of

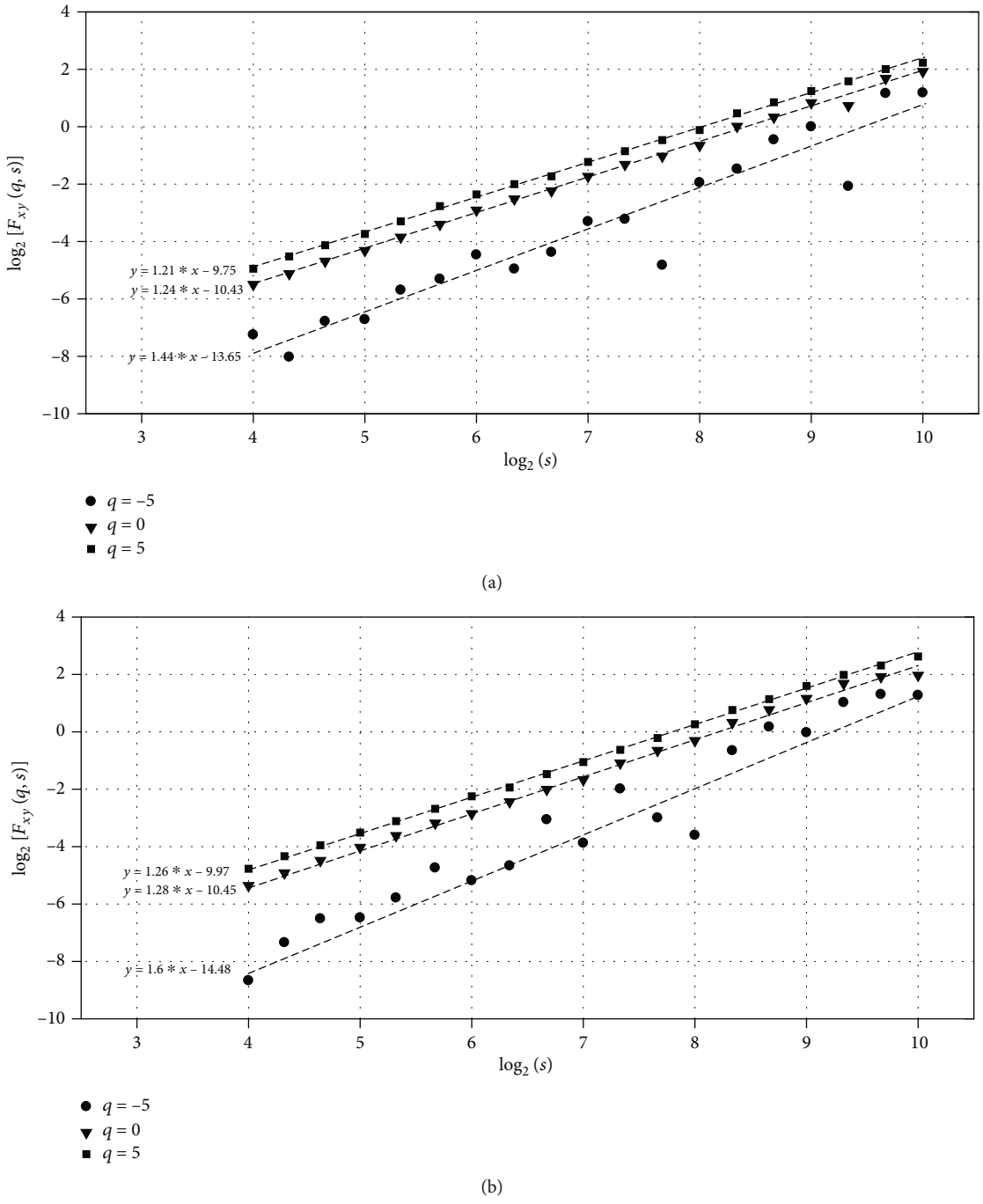

FIGURE 7: Trend of $\log_2[F_{xy}(q,s)]$ vs $\log_2[s]$ for $q = -5, 0, 5$, calculated for a particular range of η values and their corresponding φ values for (a) 8 TeV dataset and (b) 7 TeV dataset.

detrended covariance between φ values and their corresponding η values for different values of q gives a range of $h_{x,y}(q)$ forming the multifractal cross-correlation spectrum.

Figures 7(a) and 7(b) show that the q^{th} order detrended covariance or $F_{xy}(q,s)$ calculated for large values of a particular η space and its corresponding ϕ space having large values is fluctuating more with increasing scale (s) for negative values of q yielding to comparatively higher values of $h_{xy}(q)$—power-law coefficient. Also, for $q > 0$, $F_{xy}(q,s)$ would flatten or change in almost constant rate with s as evident in the figures and yielding to comparatively lesser values of $h_{xy}(q)$ for both 8 and 7 TeV energies. For calculating the degree of multifractal cross-correlation denoted by γ_is, the trend of $F_{xy}(q,s) \propto s^{hxy(q)}$ for $q = 2$ is analyzed [20], as elaborated in Section 3.2. Further, in most of the

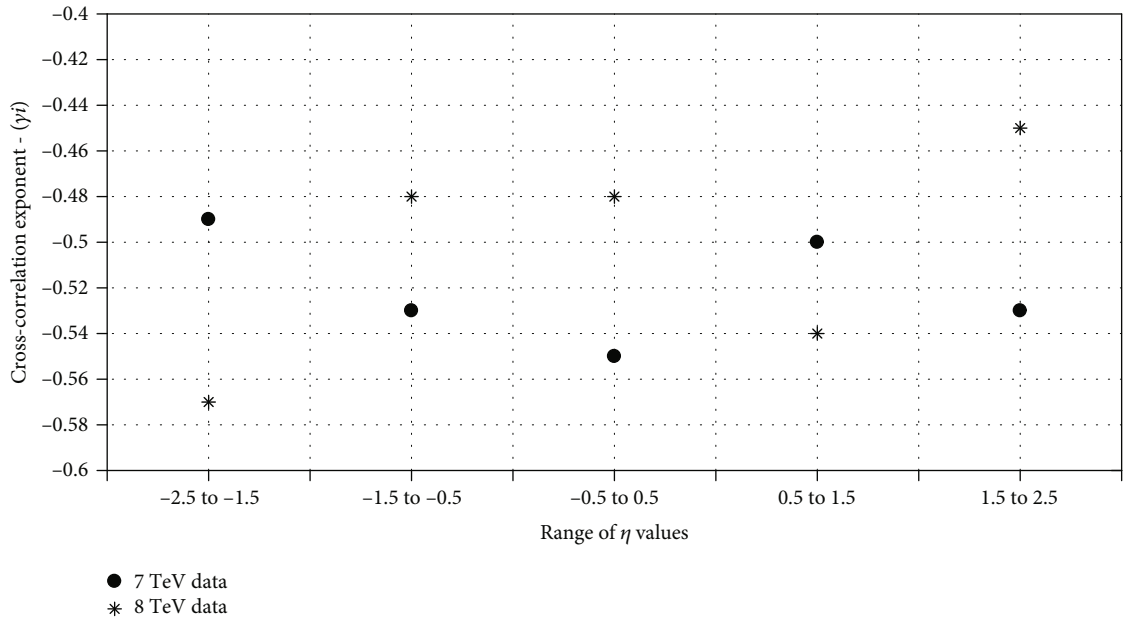

Figure 8: Comparison of multifractal cross-correlation coefficient (γ_i) between φ and η spaces for all the 5 ranges of η values for 7 and 8 TeV datasets.

Table 2: Comparison of the experimental values of multifractal cross-correlation coefficients (γ_i) between ϕ and η spaces for all the 5 ranges of η values for 7 and 8 TeV datasets, between the original and the randomized version.

η ranges	MFD-XA coefficients (γ_i)			
	8 TeV		7 TeV	
	Orig	Rand	Orig	Rand
−2.5 to −1.5	−0.57	1.01	−0.49	0.94
−1.5 to −0.5	−0.48	1.00	−0.53	0.99
−0.5 to 0.5	−0.48	1.02	−0.55	1.00
0.5 to 1.5	−0.54	0.98	−0.50	1.01
1.5 to 2.5	−0.45	0.96	−0.53	0.94

previous works, it had been shown that $F_{xy}(q, s)$ varies with increasing values of scale or s in log scale for different order or values of q, in similar manner as it is varying in this experiment.

(9) Two sets of multifractal cross-correlation coefficient, denoted by γ_i for $i = 1, 2, \cdots, 5$ for each of the 8 and 7 TeV datasets, are computed as per the method described in Section 3.2. This way, the degree of cross-correlation between ϕ and η spaces for all the 5 ranges of η values as specified in Step 1 for both 8 and 7 TeV datasets are calculated

(10) Then, each of the azimuthal ϕ spaces extracted in Step 4 is randomized, and the multifractal cross-correlation coefficients between the randomized ϕ spaces and the corresponding η spaces are extracted for both 8 and 7 TeV datasets are calculated as per the method described in Section 3.2

(11) Figure 8 shows the comparison of multifractal cross-correlation coefficients (γ_i) between ϕ and η spaces for all the 5 ranges of η values for 7 and 8 TeV datasets with respect to their rapidity as well as energy dependence. Here, we notice that:

(i) For both 7 and 8 TeV data, all the 5 η spaces are highly cross-correlated with their corresponding ϕ spaces

(ii) It should be noted that $\gamma_i = 1$ for uncorrelated data series. The more correlated the data series are, the lower the value of γ_i. For 8 TeV data, the first range of η values is most cross-correlated with the corresponding ϕ space, and the most cross-correlated range for 7 TeV data is the third one

The comparison of γ_is for all the 5 η ranges for 7 and 8 TeV datasets between the original and the randomized version is shown in Table 2. The values of the parameter, γ_i, calculated for experimental data being significantly different from the shuffled ensembles, confirm that this inherent degree of multifractal cross-correlation between each η space and its corresponding ϕ space is never the outcome of randomization process but is indicative of the inherent multifractal cross-correlation among η and corresponding ϕ values in the di-muon production process.

(12) Hence, the values of γ_is calculated for the original and the randomized version differ substantially, clearly establishing the statistical significance of the results obtained from the actual data.

5. Conclusion

Oppositely charged di-muon production is the outcome of several hypothetical processes and investigation for such processes have been the goal of experiment of *pp* collision at 7 and 8 TeV and also at other energies at the CMS collaboration. However, the present investigation, as we have pointed out earlier, is based on a deep-rooted dynamics of di-lepton production process in hadron-hadron interaction from the basic perspective of symmetry-based scaling in different pseudorapidity ranges in two different energies. We have used two rigorous and robust methodologies, namely, MF-DFA and MF-DXA, for the scaling analysis of the dynamics of the di-muon production process using di-muon data taken from the primary dataset of RunA(2011) and RunB(2012) of the *pp* collision at 7 TeV and 8 TeV, respectively, from CMS collaboration. We have analyzed how this scaling pattern has evolved from one rapidity range to the next one and how this change evolved from lower energy range of 7 TeV to the higher one 8 TeV, and the findings are listed below.

(1) The linear trend of $F_q(s)$ vs s for all the values of q for all the 5 ranges of η values for 8 and 7 TeV datasets confirms the fractality as well as the multifractality of all the pseudorapidity spaces. Figures 1(a) and 1(b) show similar trend for a particular range of η values for both energy ranges. Similar linear trend is observed for the ϕ spaces corresponding to the η spaces, which again confirm the fractality and the multifractality of the ϕ spaces as well. Figures 4(a) and 4(b) show the linear trend calculated for the ϕ spaces corresponding to the particular η range for both energy ranges

(2) Table 1 and Figure 3 show how the widths of the multifractal spectrum differ from one η space to the other and how they in turn differ from one energy range to another. It is interesting to note that for both 7 and 8 TeV energies, the η space corresponding to the first range of η has the maximum width of multifractal spectrum/degree of complexity, or in other words, they are most multifractal in nature among the other five ranges. Moreover, they have exactly the same value for the parameter. As for the minimum width of multifractal spectrum, the second η range for 8 TeV data and third η range for 7 TeV data is 0.02 which is again the same for both energy ranges

(3) The linear trend of $\log_2[F_{xy}(q,s)]$ vs $\log_2 s$ for $q = -5, 0, 5$ which is shown in Figures 7(a) and 7(b) for 8 and 7 TeV datasets, respectively, for the same specific η range and its corresponding ϕ space confirms the self-similar cross-correlation between the spaces which is evident from the goodness-of-fit for all the values of q. Similar trend is observed for the rest of the η ranges

(4) Table 2 and the Figure 8 show that for both 7 and 8 TeV data, all the 5 η spaces are highly cross-correlated with their corresponding ϕ spaces and how the degree of cross-correlation changes from one η space to the other and from one energy range to another. It should be noted that the degree of multifractal cross-correlation, γ_i, is maximum for the first η range for 8 TeV data, and the same is maximum for the third range of 7 TeV data. γ_i is minimum for the fifth η range for 8 TeV data and for the first range of 7 TeV data

This analysis manifests different degree of symmetry scaling or scale-freeness in different pseudorapidity domains and at the same time different degree of cross-correlation between pseudorapidity and azimuthal space at both energy. The differences in the values of scaling and cross-correlation exponents representing the *degree of symmetry scaling* and *degree of cross-correlation*, respectively, calculated for different ranges of rapidity and at two different energy values, indicate the existence of several processes involved in the production process of oppositely charged di-muons giving rise to varying *degree* of scaling. The observed difference of *degree of symmetry scaling* in different rapidity domains at two different energy values may provide a clue for exploring other processes in regards to di-muon production even from the perspective beyond the standard model. This novel method has the prospect for applications in different high-energy interactions to detect not only different possible resonance states but also for identification of exotic resonance states proposed by theories.

Data Availability

The data used to support the findings of this study are included within the submitted article in Section 3.1, which says the data used in the experiment is extracted from pp collision at 8 and 7 TeV of the CMS collaboration. The DOI and other details are given in the manuscript. The data is publicly available for experiment by CMS (CERN Opendata).

Conflicts of Interest

The authors declare that they have no conflicts of interest.

Acknowledgments

We thank the Department of Higher Education, Govt. of West Bengal, India for logistics support of computational analysis.

References

[1] A. Bialas and R. Peschanski, "Moments of rapidity distributions as a measure of short-range fluctuations in high-energy collisions," *Nuclear Physics B*, vol. 273, no. 3-4, pp. 703–718, 1986.

[2] A. Bialas and R. Peschanski, "Intermittency in multiparticle production at high energy," *Nuclear Physics B*, vol. 308, no. 4, pp. 857–867, 1988.

[3] E. A. De Wolf, I. M. Dremin, and W. Kittel, "Scaling laws for density correlations and fluctuations in multiparticle dynamics," *Physics Reports*, vol. 270, no. 1-2, pp. 1–141, 1996.

[4] R. C. Hwa, "Fractal measures in multiparticle production," *Physical Review D*, vol. 41, no. 5, pp. 1456–1462, 1990.

[5] G. Paladin and A. Vulpiani, "Anomalous scaling laws in multifractal objects," *Physics Reports*, vol. 156, no. 4, pp. 147–225, 1987.

[6] P. Grassberger and I. Procaccia, "Dimensions and entropies of strange attractors from a fluctuating dynamics approach," *Physica D: Nonlinear Phenomena*, vol. 13, no. 1-2, pp. 34–54, 1984.

[7] T. C. Halsey, M. H. Jensen, L. P. Kadanoff, I. Procaccia, and B. I. Shraiman, "Fractal measures and their singularities the characterization of strange sets," *Physical Review A*, vol. 33, no. 2, pp. 1141–1151, 1986.

[8] F. Takagi, "Multifractal structure of multiplicity distribution in particle collisions at high energies," *Physical Review Letters*, vol. 72, no. 1, pp. 32–35, 1994.

[9] C. K. Peng, S. V. Buldyrev, S. Havlin, M. Simons, H. E. Stanley, and A. L. Goldberger, "Mosaic organization of DNA nucleotides," *Physical Review E*, vol. 49, no. 2, pp. 1685–1689, 1994.

[10] J. W. Kantelhardt, S. A. Zschiegner, E. Koscielny-Bunde, S. Havlin, A. Bunde, and H. E. Stanley, "Multifractal detrended fluctuation analysis of nonstationary time series," *Physica A: Statistical Mechanics and its Applications*, vol. 316, no. 1-4, pp. 87–114, 2002.

[11] UA1 Collaboration, "Multifractal analysis of minimum bias events in $\sqrt{s} = 630$ $\boldsymbol{GeV}$ $\bar{p}\,p$ collisions," *Zeitschrift für Physik C Particles and Fields*, vol. 56, pp. 37–46, 1992.

[12] M. K. Suleymanov, M. Sumbera, and I. Zborovsky, *Entropy and Multifractal Analysis of Multiplicity Distributions from Pp Simulated Events up to LHC Energies*, 2003.

[13] Y. X. ZHANG, W. Y. QIAN, and C. B. YANG, "Multifractal structure of pseudorapidity and azimuthal distributions of the shower particles in Au + Au collisions," *International Journal of Modern Physics A*, vol. 18, pp. 2809–2816, 2007.

[14] E. G. Ferreiro and C. Pajares, "High multiplicity *pp* events and J/ψ production at energies available at the CERN Large Hadron Collider," *Physical Review C*, vol. 86, no. 3, 2012.

[15] M. V. Tokarev, T. G. Dedovich, and I. Zborovský, "Self-similarity of Jet and Top-quark production at Tevatron and LHC," in *Particle Physics at the Year of Centenary of Bruno Pontecorvo*, pp. 186–190, 2015.

[16] M. Tokarev and I. Zborovský, "Self-similarity of strangeness production in pp collisions at RHIC," *Journal of Physics: Conference Series*, vol. 668, 2016.

[17] M. V. Tokarev and I. Zborovský, "Self-similarity of proton spin and asymmetry of jet production," *Physics of Particles and Nuclei Letters*, vol. 12, no. 2, pp. 214–220, 2015.

[18] E. G. Baldina and A. A. Baldin, "Relativistically invariant self-similarity approach for description of collective phenomena," *EPJ Web of Conferences*, vol. 138, 2017.

[19] T. Sonoda, *Application of self-similar symmetry model to dark energy*, Preprint, 2018.

[20] B. Podobnik and H. E. Stanley, "Detrended crosscorrelation analysis: a new method for analyzing two nonstationary time series," *Physical Review Letters*, vol. 100, no. 8, 2008.

[21] F. Wang, G. P. Liao, X. Y. Zhou, and W. Shi, "Multifractal detrended cross-correlation analysis for power markets," *Nonlinear Dynamics*, vol. 72, no. 1-2, pp. 353–363, 2013.

[22] S. Bhaduri and D. Ghosh, "Pion fluctuation in high-energy collisions — a chaos-based quantitative estimation with visibility graph technique," *Acta Physica Polonica B*, vol. 48, no. 4, p. 741, 2017.

[23] ALICE-Collaboration, *Pb-Pb VSD masterclass data sample at 2.76 TeV per nucleon pair*, CERN, 2014.

[24] S. Bhaduri, A. Bhaduri, and D. Ghosh, "Pion fluctuation study in Pb–Pb collision at 2.76 TeV per nucleon pair from ALICE experiment with chaos and complex network-based methods," *Physics of Particles and Nuclei Letters*, vol. 16, no. 3, pp. 229–239, 2019.

[25] S. Bhaduri, A. Bhaduri, and D. Ghosh, *Pion Fluctuation Study in Pb-Pb Collision at 3.5TeV from ALICE Experiment with Chaos and Complex Network-based Methods*, Technical Report, 2018.

[26] S. Bhaduri, A. Bhaduri, and D. Ghosh, "Symmetry-scaling based complex network approach to explore exotic hadronic states in high-energy collision," *Physics of Particles and Nuclei Letters*, vol. 16, no. 6, pp. 779–788, 2019.

[27] S. Bhaduri and D. Ghosh, "Multiplicity fluctuation and phase transition in high-energy collision — a chaos-based study with complex network perspective," *International Journal of Modern Physics A*, vol. 31, no. 35, p. 1650185, 2016.

[28] S. Bhaduri, A. Bhaduri, and D. Ghosh, "Study of multiplicity dependence of pion fluctuations in π^-–AgBr collisions at 350 GeV using complex network approach," *Pramana-Journal of Physics*, vol. 92, no. 1, 2019.

[29] A. Bhaduri and D. Ghosh, "Quantitative assessment of heart rate dynamics during meditation: an ECG based study with Multi-Fractality and visibility graph," *Frontiers in Physiology*, vol. 7, 2016.

[30] S. Bhaduri and D. Ghosh, "Fractal study of pion void probability distribution in ultrarelativistic nuclear collision and its target dependence," *Modern Physics Letters A*, vol. 31, no. 27, p. 1650158, 2016.

[31] A. Bhaduri, S. Bhaduri, and D. Ghosh, "Azimuthal pion fluctuation in ultra relativistic nuclear collisions and centrality dependence—a study with chaos based complex network analysis," *Physics of Particles and Nuclei Letters*, vol. 14, no. 4, pp. 576–583, 2017.

[32] S. Bhaduri, A. Bhaduri, and D. Ghosh, "A new approach of chaos and complex network method to study fluctuation and phase transition in nuclear collision at high energy," *The European Physical Journal A*, vol. 53, no. 6, 2017.

[33] S. Bhaduri, A. Bhaduri, and D. Ghosh, "Clan-Model of particle production process-revisited in chaos-based complex network scenario," *Physics of Particles and Nuclei Letters*, vol. 15, no. 4, pp. 446–455, 2018.

[34] L. Zhao, W. Li, C. Yang et al., "Multifractal and network analysis of phase transition," *PLoS One*, vol. 12, p. 23, 2016.

[35] G. F. Zebende, M. V. S. da Silva, A. C. P. Rosa, A. S. Alves, J. C. O. de Jesus, and M. A. Moret, "Studying long-range correlations in a liquid-vapor-phase transition," *Physica A: Statistical Mechanics and its Applications*, vol. 342, no. 1-2, pp. 322–328, 2004.

[36] CMS Collaboration, "Search for supersymmetry in events with opposite-sign dileptons and missing transverse energy using an artificial neural network," *Physical Review D*, vol. 87, no. 7, 2013.

[37] A. Uras, "Low-mass dimuon measurements in pp, p-Pb and Pb-Pb collisions with ALICE at the LHC," *Journal of Physics: Conference Series*, vol. 668, 2016.

[38] The ATLAS Collaboration, "Measurement of the exclusive $\gamma\gamma \longrightarrow \mu^+\mu^-$ process in proton–proton collisions at $\sqrt{s} = 13$ TeV with the ATLAS detector," *Physics Letters B*, vol. 777, pp. 303–323, 2018.

[39] K. Werner, A. G. Knospe, C. Markert et al., "Resonance production in high energy collisions from small to big systems," *EPJ Web of Conferences*, vol. 171, 2018.

[40] CMS-collaboration, *MuOniaParked primary dataset in AOD format from Run of 2012 (/MuOniaParked/Run2012B-22Jan2013-v1/AOD)*, CERN, 2017.

[41] CMS-collaboration, *MuOnia primary dataset in AOD format from RunA of 2011 (/MuOnia/Run2011A-12Oct2013-v1/AOD)*, CERN, 2016.

[42] J. W. Kantelhardt, E. Koscielny-Bunde, H. H. A. Rego, S. Havlin, and A. Bunde, "Detecting long-range correlations with detrended fluctuation analysis," *Physica A*, vol. 295, no. 3-4, pp. 441–454, 2001.

[43] Y. Ashkenazy, S. Havlin, P. C. Ivanov, C. K. Peng, V. Schulte-Frohlinde, and H. E. Stanley, "Magnitude and sign scaling in power-law correlated time series," *Physica A: Statistical Mechanics and its Applications*, vol. 323, pp. 19–41, 2003.